Determining the Hierarchical Architecture of the Human Brain Using Subject-Level Clustering of Functional Networks

Teddy J. Akiki[1,2] and Chadi G. Abdallah[1,2]

[1] *National Center for PTSD – Clinical Neurosciences Division, US Department of Veterans Affairs, West Haven, Connecticut*

[2] *Department of Psychiatry, Yale University School of Medicine, New Haven, Connecticut*

Corresponding author: Chadi G. Abdallah, chadi.abdallah@yale.edu

June 19, 2018

Abstract

Optimal integration and segregation of neuronal connections are necessary for efficient large-scale network communication between distributed cortical regions while allowing for modular specialization. This network dynamic is enabled at the cortical mesoscale by the organization of nodes into communities. Previous *in vivo* efforts to map the mesoscale architecture in humans had several limitations. Here we characterize a consensus multiresolution mesoscale organization of the functional cortical network. We derive this consensus from the clustering of subject-level networks. We show that this subject-derived consensus framework yields clusters that better map to the individual, compared to the widely-used group-derived consensus approach. We also show that using clustering methods tailored for correlation networks results in functional communities that better fit anatomical metadata. We applied this analysis to state of the art magnetic resonance imaging data from 1003 healthy individuals part of the Human Connectome Project. The hierarchical atlas will be made publicly available for future investigators.

1 Introduction

Using surrogates of brain activity such as the blood-oxygen-level dependent (BOLD) signal obtained using functional magnetic resonance imaging (fMRI), whole-brain functional networks (i.e., *connectomes*) can be estimated *in vivo*. The brain functional connectome is organized at multiple spatial scales, one of which is the *mesoscale* . It has been recently shown that a full repertoire of functional communities—groups of nodes that are densely connected internally—can be consistently decoded, even at rest. In the brain, these communities are known to represent subsystems and parallel distinct neurophysiological functions (e.g., the brain's visual subnetwork)[1,2,3]. Moreover, this scale is highly sensitive to disease, where several psychiatric disorders have shown selective disruption in particular brain communities[4,5,6,7]. This apparent importance has prompted interest in this line of investigation; while a vast wealth of knowledge has been gained from these efforts, several pitfalls remain.

To map the mesoscale architecture of the normal brain, previous studies have generally applied the community detection algorithm on a group-representative network obtained by averaging networks from a group of individuals. However, it is becoming increasingly clear that important features may be lost by such averaging

(including some that are present across individuals[8]), leading to a representation that may not resemble a true central tendency in the group[9,10,11,12].

Further, the processing of networks derived from time series (i.e., correlation networks) is challenging. First, unlike prototypical networks where edges are either present or absent, edges in correlation networks represent the magnitude of statistical association, and so are on a continuum. Second, methods that are commonly used to index association—most commonly Pearson or partial correlation—also produce negative correlations. Third, these networks contain numerous indirect dependencies by virtue of the transitivity inherent in correlations[13,14]. This is particularly salient in large networks, as these indirect effects may be compounded with higher-order interactions.

Previous investigations have generally made use of thresholds prior to analysis in order to treat functional networks like usual sparse graphs. The rationale is that the strong connections that would be retained would likely be the most relevant and least likely to be artifactual, also leading to the elimination of negative edges. Recently, the relevance of weak network edges has become increasingly recognized, as they appear to convey unique information not encoded in strong edges[15,16,17,18,19]. Further, the choice of the threshold is also challenging and can give rise to heterogeneity in the findings[20,21]. Like weak edges, negative edges (i.e., anticorrelations) have been also shown to have a strong physiological basis[22,23,24,25].

While several methods exist for community detection in networks, most are not compatible with weighted networks containing both positive and negative links of the type observed in correlation networks[26,27]. One of the most commonly used and best performing methods in community detection is the Louvain algorithm[28,29,27]. The Louvain algorithm is versatile and can be used with different null models, some of which have been extended to allow for positive and negative interactions[27]. Importantly, null models that are typically used with the Louvain algorithm are based on permutations (rewiring) of the original networks, preserving the total weight and degree while randomizing connections[30]. This is known as the Newman-Girvan (NG) null model, which has also been extended to signed networks[31,32,33]. However, such an approach is problematic in the case of correlation matrices, as it assumes that the entries are independent, thereby violating the correlation transitivity[34,35]. Therefore, the community detection may not be accurate, particularly if there is heterogeneity in the size of the communities[34]—which is known to be biologically plausible in the case of the brain.

A number of recent developments in network science and neuroimaging have paved the way for frameworks that can be used to address these challenges. Here we used the Louvain algorithm, with a null model based on random matrix theory specifically designed for correlation networks (we refer to it throughout as the RMT null model)[35]. While it was initially introduced in finance[35], it has been recently successfully applied to neurophysiological recordings[36]. This method, which does not violate transitivity, is compatible with weighted and signed networks, forgoing the need to perform any thresholding. The introduction of more efficient algorithms, of reclustering frameworks, and the increased availability of high-performance computing, have made it practical to perform the clustering at the level of the individual network. As a neuroimaging dataset, we used a recent release from the Human Connectome Project (S1200 release; March 2017)[37]. This relatively-large sample of healthy individuals consists of state-of-the-art MRI data and addresses several of the limitations present in older datasets[38,39].

We hypothesized that mapping the mesoscale of the average human cortex can be better achieved by first mapping the mesoscale in each subject and then arriving at a meaningful central tendency, rather than by the mesoscale mapping of an averaged whole brain network. To this aim, we perform the clustering at the subject level followed by a reclustering procedure to reach a population consensus mesoscale architecture (we refer to this as *subject-derived consensus*)[40,41]. We compare this subject clustering-reclustering framework to the traditional group-representative method (we refer to it as *group-derived consensus*) to assess which results in solutions that map best to the individuals' data. Finally, using anatomical diffusion networks, we assess whether the RMT correlation null model is more suited for community detection in functional MRI networks compared to the more widely used permutation null models.

2 Results

2.1 Mesoscale functional organization revealed by subject-derived consensus

We first performed the community detection at the level of the individual subjects' scans. Using the multimodal parcellation (MMP) atlas[42], regional fMRI time series were used to generate functional networks and corresponding random matrix null models. These were then used with the Louvain community detection algorithm. To index the full range of spatial resolutions, we applied the algorithm recursively: each daughter community was treated as a new network and the process was repeated until no statistically significant communities were found under the null model. Near-degeneracy of the Louvain algorithm was addressed by considering 100 runs of the algorithm and picking the most stable output before proceeding to the next hierarchical level (see 4).

This resulted in a median of 5 hierarchical levels for each subject (range $1-8$). The number of communities across all levels ranged between 2 and 134. To identify a representative partitioning for the group based on the information from the subject-level partitioning, we adopted a consensus clustering approach[40,41,43,27]. This method consists of summarizing the outputs of the subject clustering results by quantifying the number of times nodes i and j were assigned to the same partition across subjects and hierarchies and populating a co-classification matrix C_{ij} with these values. This co-classification matrix was then subjected to a recursive clustering algorithm recently introduced for multiresolution consensus reclustering[40]. This resulted in a subject-derived consensus hierarchical tree with 103 levels, ranging from 3 to 112 communities (Fig. 1a).

By means of the methods that we used, all partition solutions in the hierarchy were statistically significant under the respective null models (see 4). To identify partition solutions in the consensus hierarchy that are most expressed at the level of individual subjects, we calculated the average similarity between each consensus partition solution and the subject-level partition solutions (first averaged within each subject across hierarchies, then across subjects). This allowed us to gauge the "representativeness" of the different levels, with those corresponding to local maxima considered to be of particular importance (Fig. 1b).

To facilitate the interpretability of the modular organization, here we focus on the first local maximum yielding 6 communities (Fig. 1c). At this level, the organization consisted of an occipital community corresponding to the cortical visual system (*visual*); a community centered around the central fissure and extending to the transverse temporal gyrus, corresponding to the somatosensory, auditory, motor and supplementary cortices (*somatomotor*); a community with anterior and posterior midline components (medial prefrontal and posterior cingulate cortices) as well as a middle temporal component, collectively known as the *default mode* ; a community with nodes predominantly in the frontoparietal cortex that is more expressed in the right hemisphere (*central executive*); a cingulo-opercular community spanning the ventral part of the salience system (*ventral salience*); and a more dorsal community spanning dorsal parts of the salience system (*dorsal salience*).

Interestingly, other prominent local maxima appear to have occurred at neurobiologically relevant divisions (Fig. 2). Level 9 (11 communities) corresponds to the split of the default mode community into a midline core community and middle temporal lobe community (Fig. 2a). Level 11 (13 communities) represents the split of the auditory community from the somatomotor community (Fig. 2b). Level 17 (19 communities) represents the delineation of the language community, more expressed on the left (Fig. 2c). Level 25 (30 communities) represents a hemispheric split of the central executive community (Fig. 2d).

2.2 Subject-derived consensus preserves mesoscale features

As a control procedure to the subject-level method, here we perform the community detection on a group-representative network. We concatenated the fMRI regional time series from all participants and generated connectivity and corresponding random matrix null networks. For a meaningful comparison with the subject-level method, we iterated the hierarchical algorithm an equal number of times as the subject-level method

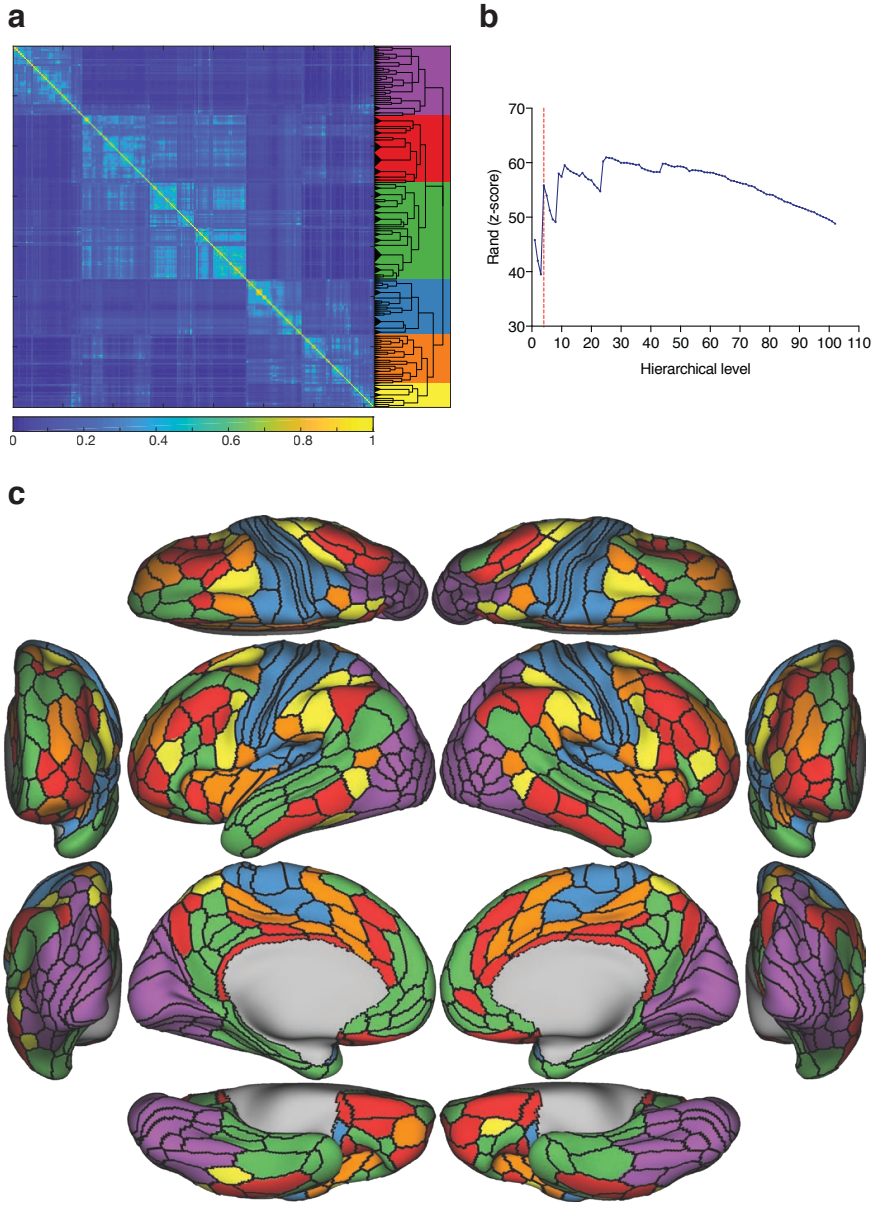

Figure 1: **Subject-derived consensus hierarchical partitioning.** (a) Co-classification matrix summarizing the results of the subject-level clustering, sorted by community affiliation. Dendrogram represents the hierarchical organization of the nested communities. The length of the arms of the dendrogram are proportional to the average value of the local null model. The background colors represent the candidate division (see below). (b) Similarity plot showing the mean similarity between the partitioning in each hierarchical level in the dendrogram and the clustering at the subject-level quantified by the z-score of the Rand coefficient. The local maximum in similarity at level 4 (dashed red line) corresponds to the partitioning of the cortex into 6 communities. (c) Brain surface plots of the 6 communities corresponding to the local maximum: visual (purple); somatomotor (blue); default mode (green); central executive (red); ventral salience (orange); and dorsal salience (yellow).

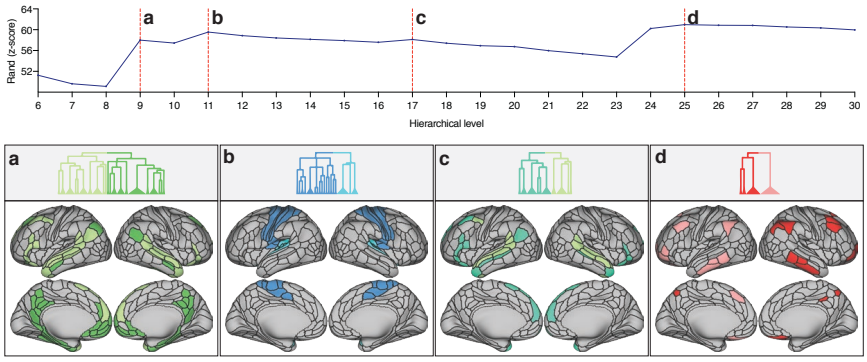

Figure 2: **Emerging communities at local maxima in the subject-derived consensus hierarchical partitioning.** Top: similarity plot showing the mean similarity between the partitioning in each hierarchical level and the clustering at the subject-level quantified by the z-score of the Rand coefficient. The local maxima in similarity are denoted by the dashed red lines. Bottom: (a) Level 9 is characterized by splitting of the default mode community into a midline core community (dark green) and middle temporal lobe community (light green), compared to the preceding level. (b) Level 11 is characterized by the splitting of the auditory community (light blue) from the somatomotor community (dark blue). (c) Level 17 is characterized by the emergence of the language community (turqoise) from lateral default mode (light green). (d) Level 25 is characterized by the hemispheric split of the left and right central executive community (red and pink).

(1003 times) and used the multiresolution output from these runs to populate a co-classification matrix. Since the first-level clustering here was performed on a single group-representative network, a slight variability in the outputs of the 1003 runs was deemed necessary to achieve a rich co-classification matrix. For this reason, the procedure to control for the near-degeneracy was applied at the hierarchical consensus clustering only (see 4). Each run resulted with a median of 5 hierarchical levels (range $4-5$). We then built a co-classification matrix C_{ij} using the outputs and performed the hierarchical consensus reclustering step. This resulted in a group-derived consensus hierarchy of 101 levels, with a number of communities ranging between 4 and 143 (Fig. 3a).

One of the goals of this study was to assess whether applying the clustering algorithms at the subject level followed by meta-reclustering to reach a group consensus (i.e., the method in the previous section) confers a meaningful advantage over applying the clustering algorithm to a group-representative network as is generally done in the literature. For this reason, we calculated the average similarity between the group average-derived consensus partitions (Fig. 3a) and the partitions at the level of the individual subjects. We compared these values with the similarity between the subject-derived consensus partitions and the partitions at the level of the individual subjects (Fig. 3b). Compared to the group-derived consensus partitions, the subject-derived consensus partitions were more similar to the individuals' partitioning throughout the hierarchical levels in common (two sample t test, $10^{-172} < p < 10^{-4}$; Fisher's combined probability test, $p < 10^{-307}$). One exception is the partitioning that yielded 4 communities, where the group-derived consensus showed higher similarity to individuals' partitioning (two sample t test, $p < 10^{-5}$).

2.3 Clustering functional networks using RMT results in communities that are more consistent with anatomical networks

The argument against the use of the traditional Newman-Girvan permutation-based null model (of the type similar to Eq. 2) for correlation networks has been well described using synthetic and real-world data for which the ground truth organization is known[35,34]. However, this has not been specifically demonstrated to apply to fMRI data where it remains widely used. Here, we repeated the community detection using the NG

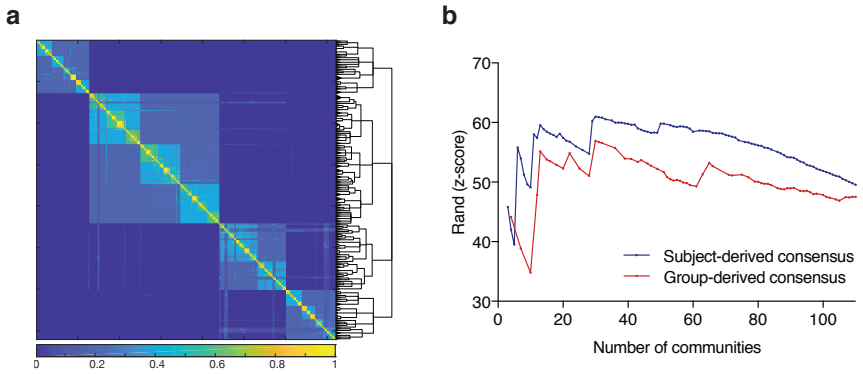

Figure 3: **Group-derived consensus hierarchical partitioning.** (a) Co-classification matrix summarizing the results of the multiple group-level clustering, sorted by community affiliation. Dendrogram represents the hierarchical organization of the nested communities. The length of the arms of the dendrogram are proportional to the average value of the local null model. (b) Similarity plot showing the mean similarity between the clustering at the subject-level, and the partitioning in each hierarchical level (here sorted by number of communities) in the group-derived consensus partitioning (red) and the subject-derived consensus partitioning (blue); quantified by the z-score of the Rand coefficient. The subject-derived consensus was more similar than the group-derived consensus across all shared levels, with one exception at the partition yielding 4 communities.

null model to contribute to this body of literature. The same community detection procedures described above were repeated here with a signed permutation null model (i.e., modularity function in Eq. 3). The result of the hierarchical partitioning can be seen in Fig. 4a.

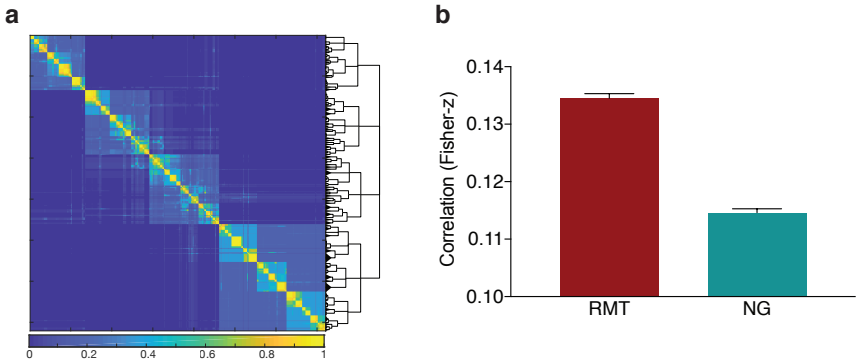

Figure 4: **Group-derived consensus hierarchical partitioning using the NG null model.** (a) Co-classification matrix summarizing the results of the multiple group-level clusterings, sorted by community affiliation. Dendrogram represents the hierarchical organization of the nested communities. The length of the arms of the dendrogram are proportional to the average value of the local null model. (b) Comparison between the mean Fisher-z transformed correlation values between the subject-level anatomical networks, RMT co-classification matrix (red) and the NG co-classification matrix (teal); the error bars represent the 95% confidence interval.

In the absence of ground truth knowledge of the network organization in the human brain, the evaluation of the results obtained from the clustering using the RMT vs. NG null model becomes challenging. To evaluate it using the subjects' correlation networks would not only be circular, but also implicates the same transitive

bias we set out to avoid[34,13]. To this end, we instead used tractography to reconstruct anatomical networks from diffusion MRI. While there's no direct correspondence between the two, anatomical connections are known to shape functional connections[44,45,46]. Thus, we considered that the overall functional clustering results that best approximate the anatomical networks would indicate a favorable performance of the null model[47,48].

We calculated Spearman's correlations between the individual anatomical networks and the zero-centered co-classification matrices derived using the RMT and the NG null models. The Fisher-z transformed correlation values were then compared across the two methods. In both cases, anatomical networks were only weakly correlated with co-classification matrices (mean Fisher-z $r_s = 0.125$). Compared to NG, the co-classification matrix corresponding to the RMT was more correlated to anatomical networks (two-tailed t test, $p < 10^{-229}$) (Fig. 4b). For robustness, we also attempted to match the co-classification matrices in terms of binary density by using a proportional threshold, which yielded a similar result. Further analyses conducted were consistent with this finding and can be found in the supplement.

3 Discussion

Using subject-level clustering of functional networks and a reclustering framework, we mapped the mesoscale architecture of the cortex at multiple scales. Confirming the study hypothesis, the subject-derived consensus framework yielded results that were more similar to the individual subjects compared to the group-derived consensus, despite the fact that both were obtained from the same starting data. While it is inevitable that any type of average will obscure individual features, obtaining a population-level representation that is as faithful as possible to the mesoscale of individuals is preferable. The subject-level consensus enables a representation that better represents a central tendency, resembling individuals to a greater extent.

In previous studies, resting-state fMRI acquisitions typically consisted of few minutes (e.g., 5–10 min; TR = 3,000 ms), therefore, averaging may have been a good strategy to increase the signal-to-noise ratio. However, in the current study, the acquisitions consisted of 60 min (TR = 720 ms) potentially mitigating this issue. The implicit assumption that the individual subjects' clustering results are an appropriate reference is reinforced by a body of literature showing that subject-per-subject extraction of community organization better agrees with the individuals' behavioral characteristics[49].

Several important neuroanatomical observations can be made. The representative partition solution that yielded 6 clusters (level 4; Fig. 1c) corresponds to a well described set of functional systems[1,2]. The visual system can be seen represented in a large occipital, ranging from early and higher order visual cortices to the dorsal and ventral streams. At finer divisions, they separate into a distinct early visual cortex and ventral and dorsal stream communities, as well as other visual-multimodal communities. Even at the coarsest scale, the visual system comprised a separate community than the somatosensory system. Likely, a parallel of the heavy anatomical differentiation in that area and consistent with electrophysiological studies in humans and primates[50]. The somatomotor community included both early and higher somatosensory and motor cortices, and the supplementary motor cortex. Relatively early on in the hierarchy, there is a separation of the auditory system (level 11; Fig. 2b). The rest of the somatomotor system remains relatively cohesive. The cluster that spans several midline (medial prefrontal cortex and posterior cingulate cortex) and middle temporal structures, is known in the literature as the default mode, and is known to be involved in task-negative processes[51]. At level 4 (Fig. 1c), the default mode constitutes a single entity, but subsequently branches into a midline cluster (anterior medial prefrontal and posterior cingulate cortices) and a middle temporal cluster (Level 9; Fig. 2a). This division is consistent both functionally and anatomically; evidence from task-imaging showing that the midline structures are functionally specialized in self-relevant decisions and the inference of other people's mental states (i.e., theory of mind), whereas the temporal components are implicated in autobiographical memory[51]. A single community at level 2 (4 communities; Fig. 1a) that is spread over several higher order associative regions implicated in salience detection and response, subsequently branches

into specialized ventral (also known as the cingulo-opercular system) and dorsal salience systems (Fig. 1c), an organization that has been well described previously[52].

Interestingly, at level 17 (Fig. 2c), there is branching of a community that is mostly expressed on the left hemisphere and includes Broca's area and the superior temporal gyrus, and bears striking resemblance to areas of activation during language processing task (Fig. S2). This community, which has traditionally evaded most mesoscale investigations[1,2], may represent a language system.

In general, the communities were widely distributed spatially. This is possibly due to the fact that functional communication carries relatively little cost to the organism, compared to structural connections which requires heavy investment in neuronal wiring and where communities are usually found to be spatially contiguous (though a bias against long-range/interhemispheric connections in tractography algorithms could also contribute to this)[48,53].

Another interesting observation is the absence of a parallel to the "limbic" network described by Yeo et al. which was localized to the ventral surface of the brain[1]. A possible explanation is that the older data that was used in their study had marked signal dropout at the base of the brain, where this network was identified. The HCP data used in the current study had significant improvements in terms of a reduction in signal dropout from the ventral brain and other regions due to air sinuses; notably the orbitofrontal, inferior temporal, and lateral mid-temporal cortices[54]. In our analyses, parcels in this region were assigned to the default mode and the central executive communities. Another possible explanation for this discrepancy could be the varying definition of what a "cluster" means across studies. Here clusters refer to communities, whereas in the Yeo et al. study, clusters were identified based on connectivity profiles[1].

Functional connections are thought to be shaped by an underlying anatomical network[44,45,46], though there is no one-to-one correspondence between the two; functional networks are more dynamic and vary on a much shorter timescale. Our rationale was that *real* functional networks should agree more with anatomy, compared to *measured* functional networks which are subject to transitive information flow. This inherent problem which arises because of the way functional networks are estimated from correlations, results in artifactual connections due to second-, third- and higher-order interactions that are not present in the real direct network. For example, if nodes 1 and 2 and nodes 1 and 3 are strongly correlated, a correlation will also be observed between node 2 and 3 even where none exists (or, if a true relationship exists, here it would be overestimated). This leads to inaccurate estimation of the network structure. The community detection method that we employed mitigates these effects, and so we wanted to see whether the unbiased community configuration is closer to the anatomical network which we considered to be a surrogate for ground truth. Our results indicate that the RMT clustering better maps to anatomy, likely by being devoid of this bias. In a recent study, NG failed to recover the ground truth community from neurophysiological recordings in the suprachiasmatic nucleus in mice, while an RMT null model was successful[36]. Another null model which can be used with correlation networks is known as the uniform null model[55,56,34]. However, in our application it results in a large number of singleton communities.

Limitations: In this study, we constrained the analysis to the cerebral cortex, though we recognize the importance of extending the mapping of these communities to the subcortex and cerebellum. The multimodal brain atlas that we adopted does not include any subcortical or cerebellar nodes. However, it is believed to be the most neuroanatomically accurate to date[42], although it should be noted that other—perhaps more functionally coherent—atlases exist[57,58]. Some groups have added community affiliations for the subcortex or cerebellum on a post hoc basis[59,60]. The challenge in our case is to keep the definition of a community consistent. This will likely require the treatment of the nodes of the whole brain at the same time. Finally, other mesoscale organizations should also be explored, such methods include stochastic block modeling and overlapping communities[61]. For example, using stochastic block modeling has been recently shown to more varied types of communities in the structural connectome, including core-periphery and disassortative communities[48]. We estimated the functional networks from the whole resting-state fMRI acquisition. This prevents observations regarding temporal dynamics, which should be pursued in future studies.

4 Methods

4.1 Neuroimaging dataset

The data that we use in this work is from the Washington University-Minnesota Consortium Human Connectome Project (HCP)[37]. The latest release at the time of writing was adopted (S1200; March 2017). Details regarding this dataset have been previously published[37,39]. Briefly, it included state-of-the-art whole-brain MRI acquisition with structural, functional, and diffusion-weighted imaging; the scanner was a customized Siemens Skyra 3T scanner with slice-accelerated sequences for fMRI[62,63,64,65,38]. Whole-brain functional data were acquired in two sessions. Each session consisted of two phase-encoding directions (left-right and right-left) each a 15 min multiband gradient echo-planar resting-state run (Voxel size = 2.0 x 2.0 x 2.0 mm; TR = 720 ms; TE = 33.1 ms; Flip angle = 52°; 72 slices; Bandwidth = 2,290 Hz/pixel; FOV = 208 x 180 mm). Informed consents were obtained from all subjects. The study procedures were approved by the institutional review boards. This release includes 1097 subjects with resting-state fMRI scans. Our analysis was restricted to subjects who completed all four resting-state scan runs; namely, two sessions, each with two encoding runs. This resulted in n = 1003 individuals; 534 females and 469 males. The age range was 22 to 37, with a mean of 28.7.

4.2 First-level processing

The HCP minimal processing pipeline was used[66,65]. Briefly, this included projection to the surface space, 2 mm FWHM smoothing, ICA+FIX denoising with minimal high-pass filtering[67,68], and MSMall surface registration[69,70,71]. To define our ROIs, we used a newly-developed multimodal parcellation[42]. We chose this parcellation because it is neuroanatomically informed, with data from cortical architecture (including cortical folding, thickness, and myelin maps), connectivity, and topography. This parcellation consisted of 360 ROIs (180 per hemisphere) that cover the entirety of the cerebral cortex. In the standard surface space, we calculated the mean time series from all voxels within each ROI. Resting-state fMRI time courses from the left-right and right-left phase-encoding runs and the two sessions were concatenated (total duration 60 minutes; 4800 time point). Functional connections between nodes i and j were defined as the Fisher-z transformed Pearson product-moment correlation of their respective time series.

4.3 Community detection

This consisted of using the Louvain community detection algorithm[28]; specifically, an iterated version as implemented in the GenLouvain package[72]. This versatile method is based on finding communities with a high degree of intra- and low degree of inter- connectedness. This is achieved heuristically by optimizing the modularity metric Q , which captures the degree of connectedness within communities compared to connectedness expected under a null model [28,30]:

$$Q = \frac{1}{2m} \sum_{ij} \left[A_{ij} - P_{ij}\right] \delta\left(c_i, c_j\right) \tag{1}$$

where A and P are the observed and null adjacency matrices, respectively; and $m = \frac{1}{2}\sum_{ij} A_{ij}$ is the total strength of the network. The Kronecker $\delta\left(c_i, c_j\right)$ function is equal to 1 when i and j are in the same community and 0 otherwise. As mentioned in the introduction, classical formulation of P is that of a permutation null model[30]:

$$P_{ij} = \frac{s_i s_j}{2m} \tag{2}$$

where $s_i = \sum_j A_{ij}$ is the strength of node i. Although this definition was extended to weighted signed networks[31,32,33], it remains inappropriate for use with networks generated from correlation of time series. Namely because entries in the correlation matrices are not independent, which leads to a bias in community

detection[34,35,36,13]. We avoided this by adopting a null model that was specifically designed for correlation-based networks[35] (detailed below). The networks were not thresholded, retaining all weights (both positive and negative).

Methods related to modularity maximization are known to suffer from the resolution limit—the inability to detect communities smaller than a certain size[73]. Several methods have been used to address this [74,75,26]. Here we adopt a recursive hierarchical approach to recover the community structure at multiple scales[40,76]. After detecting the first-level (i.e., coarsest) communities in the initial run of the algorithm, we define each detected community as a separate subgraph and run the algorithm recursively on each. This is repeated until no more statistically significant subcommunities can be detected. This iterative procedure allows the resolution of a hierarchically nested structure. Indeed, this is consistent with notions of ground truth hierarchical organization in the cortex from microscopic tracer studies in other mammals[50,77]. We use this hierarchical framework at the subject-level, and a slightly different one at the reclustering stages (see below).

Due to the nearly degenerate outputs of the Louvain algorithm[78], for each subject-level run, we performed 100 iterations and adopted the partition that is most similar to the ensemble, borrowing the approach from[79,80,43]. The rationale is that similarity to the ensemble can be used as a surrogate for stability, and the most stable partition solution is likely the closest to the ground truth[27,43]. To evaluate partition similarity, we used the z-score of the Rand coefficient (described below) and calculated the pairwise similarity between all 100 partition solutions, selecting for each subject the partition with the highest mean similarity to the ensemble. Since the community detection procedure was applied recursively in a hierarchical manner, 100 iterations and subsequent selection of the representative partition based on similarity was also applied to each subcommunity. This was done in order to avoid adopting an arbitrary solution from each subject.

4.4 A random matrix null model for correlation networks

To generate null models that are appropriate for use with correlation networks, we adopted a method based on random matrix theory (RMT). It is described in full detail in the original publication[35]. Briefly, this method builds null networks using a modified Wishart distribution with the same common trend and noise as the observed network, but without the community structure. This method does not require thresholding and is compatible with negative values. The end result being that positive interactions are maximally concentrated within modules and negative interactions expelled outside.

For the hierarchical recursive application, after identification of a community c in the initial network, we regenerate a null model from time series of nodes belonging to this community, and the community detection is then applied to this subgraph. One criticism of such recursive procedures relates to the fact that there are no clear stopping rules[26]. Here, it is important to mention that by virtue of the null model that we employ, only communities that are present in the RMT-filtered networks are detected[35]; therefore, the procedure stops automatically whenever no further "statistically significant" subcommunities can be detected.

4.5 Partition similarity

In order to measure the similarity between two partitions, we adopted the z-score of the Rand coefficient[79,80]. The Rand coefficient of two partitions is calculated as the ratio of the number of node pairs classified in agreement in both partitions, to the total number of pairs[81]. Here we use the z-score variant introduced in ref.[79], which can be interpreted as a measure of how similar two partitions are, beyond what might arise at random[79,27]. The z-score of the Rand coefficient between partition a and b can be written as:

$$R_{ab} = \frac{1}{\sigma_{w_{ab}}} \left(w_{ab} - \frac{M_a M_b}{M} \right)$$

Where M is the total number of node pairs, M_a and M_b the numbers of node pairs in the same community in a and b respectively, w_{ab} the number of pairs that figure in the same community in both a and b, and $\sigma_{w_{ab}}$ the standard deviation of w_{ab}.

4.6 Hierarchical consensus reclustering

Our multiresolution co-classification matrices embed information from the different hierarchical levels of community structures detected from the clustering results at the level of the subjects' networks. The recently developed consensus reclustering procedure that we adopted extends the classical formulation of consensus reclustering[41], by allowing a hierarchical multiresolution output and has built-in tests for statistical significance[40]. Here, the quality function was modularity-like as in Eq. 1, with a "local" variant of the permutation null model. Briefly, in addition to the constraint of the traditional permutation model of a fixed size and number of communities, this local model also assumes that node i is fixed and node j is random when calculating $P_{ij}^{\text{local}}(\alpha)$. This means that the null network only receives contributions from nodes that are less frequently co-classified together compared to the local permutation model, at a statistical significance level α. More detail can be found in ref.[40].

The same recursive principle and Louvain implementation described above were used here. To ensure a stable output, 100 iterations are used at each level (cases of output instability are dealt by meta-reclustering as in refs.[41,40]); the threshold for statistical significance is set at $\alpha = 0.05$.

4.7 Community detection with a permutation null model

Weighted and signed generalizations of the modularity function with the permutation null model have been previously described[31,32,33]. They take a form similar to:

$$Q^{\text{signed}} = \frac{1}{m^+}\sum_{ij}\left[A_{ij}^+ - \frac{s_i^+ s_j^+}{m^+}\right]\delta\left(c_i, c_j\right) - \frac{1}{m^-}\sum_{ij}\left[A_{ij}^- - \frac{s_i^- s_j^-}{m^-}\right]\delta\left(c_i, c_j\right) \tag{3}$$

It should be mentioned that other variants exist, such as the one introduced in ref.[32], with an asymmetrical treatment of positive and negative edges (attaching more importance to the positives); though this resulted in highly similar results in our initial testing. As this is not the primary aim of the study, we only applied this method to a group-representative matrix (i.e., group-derived consensus). We obtained an average connectivity matrix calculated by taking the subjects' Fisher z-transformed correlation matrices and taking the mean of each entry across all subjects. We then used the same procedure used for the RMT group-derived consensus to characterize the partitions at multiple scales hierarchically.

Our aim was to assess this null model using anatomical networks (see supplement for description of the data and processing). We calculated the Spearman's rank-order correlations between the zero-centered vectorized upper triangles of the co-classification matrices and the individuals' anatomical networks. The resulting coefficients were Fisher-z transformed and compared across two clustering outputs (NG vs. RMT). Additional analyses can be found in the supplement.

5 Acknowledgements

Data were provided by the Human Connectome Project, WU-Minn Consortium (Principal Investigators: David Van Essen and Kamil Ugurbil; 1U54MH091657) funded by the 16 NIH Institutes and Centers that support the NIH Blueprint for Neuroscience Research; and by the McDonnell Center for Systems Neuroscience at Washington University. Funding support was provided by the U.S. Department of Veterans Affairs National Center for PTSD and NIH (MH-101498). The content is solely the responsibility of the authors and does not necessarily represent the official views of the sponsors. We would like to thank Samaneh Nemati for data curation. We acknowledge the computational resources provided by Yale University and the National Center for PTSD.

6 Supplementary material

6.1 Anatomical data

High angular resolution diffusion MRI scans were available for a subset of same cohort from the HCP S1200 release. In the end, of the 1003 individuals we used in the fMRI analyses, 992 had successful anatomical networks. The details of the scanning procedures have been previously reported by the HCP consortium[37]. Briefly, the acquisition was conducted using a multi-shell diffusion scheme, with b-values of 1,000, 2,000, and 3,000 s/mm^2; sampling directions of 90 in each; and spatial resolution of 1.25 x 1.25 x 1.25 mm^3[37,39]. The data were subsequently corrected for motion, eddy currents, and distortions[82,83,84].

We reconstructed the diffusion data using generalized q-sampling imaging (GQI) using the DSI Studio package (http://dsi-studio.labsolver.org) with a diffusion sampling length ratio of 1.25, after the B0 volume of each subject was registered to their corresponding high resolution structural scan[85]. GQI is a model-free method that has been shown to perform well in recent benchmarks[86]. Whole brain fiber tracking was conducted using a deterministic algorithm using DSI Studio[87]. We used a total of 10,000,000 whole-brain subvoxel seeds, with an angular threshold of 55°, step size of 1.0 mm, minimum and maximum fiber length of 20 and 400 mm respectively, and a threshold of the 0.6 x Otsu for the quantitative anisotropy.

A volume-based version of the same multimodal parcellation adopted for the fMRI data was used for parcellation[42]. This atlas was dilated by 2 mm into the white matter to ensure contact between the reconstructed fibers and the brain parcels at the white-gray matter interface[88]. We counted the number of streamlines between region i and j, normalized by their parcel volumes. Normalization by parcel volume was done to account for the bias due to the fact that the volume of the regions of interest were not equal in this parcellation atlas (larger regions may have a higher probability of being in contact with a fiber streamline)[89]. The end result was an undirected weighted brain network.

6.2 Assessing RMT and NG using anatomical networks

In the absence of ground truth knowledge of the network organization in the human brain, the evaluation of the results obtained from the clustering using the null model derived from random matrix theory vs. the Newman-Girvan permutation null model becomes challenging. In the main text, we calculated correlations between co-classification matrices and anatomical networks. To ensure the robustness of the conclusion, here we follow a different approach. The total modularity Q from Eq. 1 can be expressed as a sum of the individual contributions of community c to the total modularity such that $Q = \sum_c q_c$, where

$$q_c = \frac{1}{m} \sum_{ij \in c} \left[A_{ij} - \frac{s_i s_j}{2m} \right]$$

However, because we were to compare partitions of different size and numbers, this definition would not be adequate, as communities with a larger number of nodes will naturally have a larger modularity[26,27,90]. To account for this bias, we define the standardized variant of q_c as:

$$z_{q_c} = \frac{q_c - \mu \left[q_{c_{\text{rand}}} \right]}{\sigma \left[q_{c_{\text{rand}}} \right]}$$

Where $q_{c_{\text{rand}}}$ is calculated with 5,000 random permutations to the community assignments, while keeping constant the total number and size of the communities[90,76,91]. Therefore, z_{q_c} would represent how well each functionally-identified community maps onto the anatomical networks, beyond what is expected by its size (i.e., the number of nodes it comprises) or the number of clusters. For each partition solution, the average of z_{q_c} across communities would represent how well, on average, functional communities map to anatomical networks.

For each hierarchical level derived using the two null models, we calculated the mean z_{q_c}. In all shared levels except 1 level (yielding 20 communities), the clusters derived from RMT null model better mapped to the anatomical networks than those derived from the NG null model (two sample t test, $10^{-303} < p < 3.9\times10^{-2}$; Fisher's combined probability test, $p < 10^{-307}$) (Fig. S1).

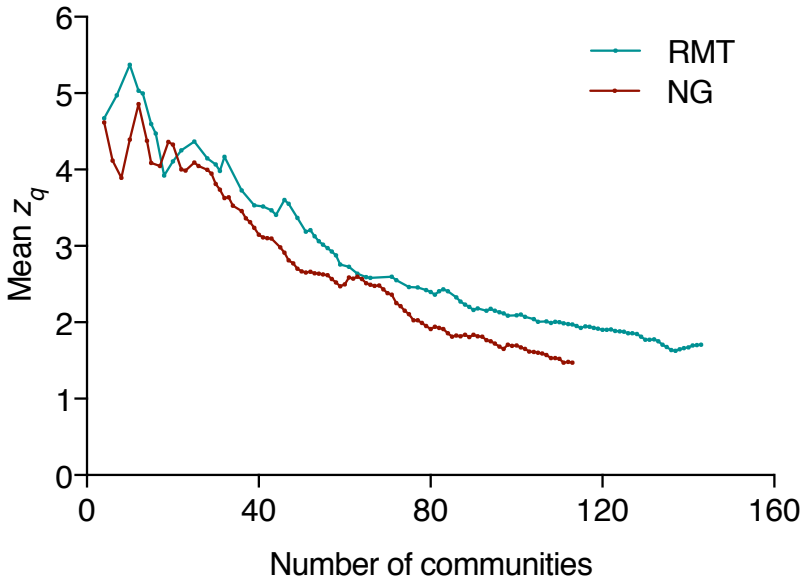

Figure S1: **Comparison between RMT and NG.** Quantitative assessment of the average partition quality z-score calculated from the anatomical diffusion networks across hierarchical levels (here sorted by number of communities) for the RMT-derived partitions (cyan) and the NG-derived partitions (red).

6.3 Assessing the putative language network

In addition to resting-state fMRI, the HCP data also included several task fMRI contrasts[92]. To visually confirm if the putative language community that we identified in the resting-state network (Fig. 2b) corresponds to language activation, we made use of the language fMRI task. Briefly, the HCP task pipeline was used to with minimal preprocessing analogous to resting-state fMRI[93,70,92]. For details see ref.[42]. The language processing task consisted of presenting brief auditory stories, and contrasted with auditory math instructions blocks of approximately equal length[92,94]. For detail see refs.[92,94]. A group average effect size contrast map for the language story vs. math task was then overlaid over putative language community, where a considerable agreement was evident (Fig. S2).

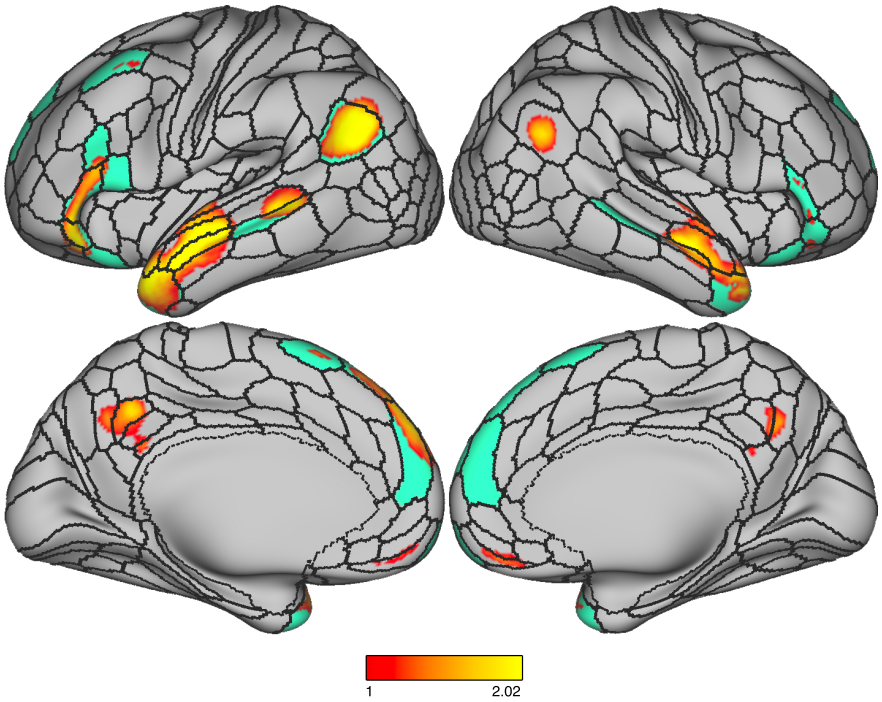

Figure S2: **Language task activation overlaid on putative language community.** Brain plots showing group average effect size contrast map for the language story vs. math task contrast (displaying activations Cohen's $d > 1$).

References

1. Yeo BTT, Krienen FM, Sepulcre J, Sabuncu MR, Lashkari D, Hollinshead M, et al. The organization of the human cerebral cortex estimated by intrinsic functional connectivity. Journal of Neurophysiology [Internet]. American Physiological Society; September 2011;106(3):1125–65. Retrieved from: https://doi.org/10.1152%2Fjn.00338.2011

2. Power JD, Cohen AL, Nelson SM, Wig GS, Barnes KA, Church JA, et al. Functional Network Organization of the Human Brain. Neuron [Internet]. Elsevier BV; November 2011;72(4):665–78. Retrieved from: https://doi.org/10.1016%2Fj.neuron.2011.09.006

3. Cole MW, Bassett DS, Power JD, Braver TS, Petersen SE. Intrinsic and Task-Evoked Network Architectures of the Human Brain. Neuron [Internet]. Elsevier BV; July 2014;83(1):238–51. Retrieved from: https://doi.org/10.1016%2Fj.neuron.2014.05.014

4. Alexander-Bloch A, Lambiotte R, Roberts B, Giedd J, Gogtay N, Bullmore E. The discovery of population differences in network community structure: New methods and applications to brain functional networks in schizophrenia. NeuroImage [Internet]. Elsevier BV; February 2012;59(4):3889–900. Retrieved from: https://doi.org/10.1016%2Fj.neuroimage.2011.11.035

5. Akiki TJ, Averill CL, Abdallah CG. A Network-Based Neurobiological Model of PTSD: Evidence From Structural and Functional Neuroimaging Studies. Current Psychiatry Reports [Internet]. Springer Nature; September 2017;19(11). Retrieved from: https://doi.org/10.1007%2Fs11920-017-0840-4

6. Akiki TJ, Averill CL, Wrocklage KM, Scott JC, Averill LA, Schweinsburg B, et al. Default mode network abnormalities in posttraumatic stress disorder: A novel network-restricted topology approach. NeuroImage [Internet]. Elsevier BV; August 2018;176:489–98. Retrieved from: https://doi.org/10.1016%2Fj.neuroimage.2018.05.005

7. Menon V. Large-scale brain networks and psychopathology: a unifying triple network model. Trends in Cognitive Sciences [Internet]. Elsevier BV; October 2011;15(10):483–506. Retrieved from: https://doi.org/10.1016%2Fj.tics.2011.08.003

8. Gordon EM, Laumann TO, Adeyemo B, Gilmore AW, Nelson SM, Dosenbach NUF, et al. Individual-specific features of brain systems identified with resting state functional correlations.. Neuroimage. 2017;146:918–39.

9. Dubois J, Adolphs R. Building a Science of Individual Differences from fMRI. Trends in Cognitive Sciences [Internet]. Elsevier BV; June 2016;20(6):425–43. Retrieved from: https://doi.org/10.1016%2Fj.tics.2016.03.014

10. Hacker CD, Laumann TO, Szrama NP, Baldassarre A, Snyder AZ, Leuthardt EC, et al. Resting state network estimation in individual subjects. NeuroImage [Internet]. Elsevier BV; November 2013;82:616–33. Retrieved from: https://doi.org/10.1016%2Fj.neuroimage.2013.05.108

11. Gordon EM, Laumann TO, Gilmore AW, Newbold DJ, Greene DJ, Berg JJ, et al. Precision Functional Mapping of Individual Human Brains. Neuron [Internet]. Elsevier BV; August 2017;95(4):791–807.e7. Retrieved from: https://doi.org/10.1016%2Fj.neuron.2017.07.011

12. Finn ES, Shen X, Scheinost D, Rosenberg MD, Huang J, Chun MM, et al. Functional connectome fingerprinting: identifying individuals using patterns of brain connectivity.. Nat Neurosci. 2015;18:1664–71.

13. Zalesky A, Fornito A, Bullmore E. On the use of correlation as a measure of network connectivity. NeuroImage [Internet]. Elsevier BV; May 2012;60(4):2096–106. Retrieved from: https://doi.org/10.1016%2Fj.neuroimage.2012.02.001

14. Giraud BG, Heumann JM, Lapedes AS. Superadditive correlation. Physical Review E [Internet]. American Physical Society (APS); May 1999;59(5):4983–91. Retrieved from: https://doi.org/10.1103%

2Fphysreve.59.4983

15. Santarnecchi E, Galli G, Polizzotto NR, Rossi A, Rossi S. Efficiency of weak brain connections support general cognitive functioning. Human Brain Mapping [Internet]. Wiley; March 2014;35(9):4566–82. Retrieved from: https://doi.org/10.1002%2Fhbm.22495

16. Lohse C, Bassett DS, Lim KO, Carlson JM. Resolving Anatomical and Functional Structure in Human Brain Organization: Identifying Mesoscale Organization in Weighted Network Representations. Fornito A, editor. PLoS Computational Biology [Internet]. Public Library of Science (PLoS); October 2014;10(10):e1003712. Retrieved from: https://doi.org/10.1371%2Fjournal.pcbi.1003712

17. Bassett DS, Nelson BG, Mueller BA, Camchong J, Lim KO. Altered resting state complexity in schizophrenia. NeuroImage [Internet]. Elsevier BV; February 2012;59(3):2196–207. Retrieved from: https://doi.org/10.1016%2Fj.neuroimage.2011.10.002

18. Gallos LK, Makse HA, Sigman M. A small world of weak ties provides optimal global integration of self-similar modules in functional brain networks. Proceedings of the National Academy of Sciences [Internet]. Proceedings of the National Academy of Sciences; February 2012;109(8):2825–30. Retrieved from: https://doi.org/10.1073%2Fpnas.1106612109

19. Goulas A, Schaefer A, Margulies DS. The strength of weak connections in the macaque cortico-cortical network. Brain Structure and Function [Internet]. Springer Nature; July 2014;220(5):2939–51. Retrieved from: https://doi.org/10.1007%2Fs00429-014-0836-3

20. Jalili M. Functional Brain Networks: Does the Choice of Dependency Estimator and Binarization Method Matter?. Scientific Reports [Internet]. Springer Nature; July 2016;6(1). Retrieved from: https://doi.org/10.1038%2Fsrep29780

21. Garrison KA, Scheinost D, Finn ES, Shen X, Constable RT. The (in)stability of functional brain network measures across thresholds. NeuroImage [Internet]. Elsevier BV; September 2015;118:651–61. Retrieved from: https://doi.org/10.1016%2Fj.neuroimage.2015.05.046

22. Fox MD, Snyder AZ, Vincent JL, Corbetta M, Essen DCV, Raichle ME. From The Cover: The human brain is intrinsically organized into dynamic anticorrelated functional networks. Proceedings of the National Academy of Sciences [Internet]. Proceedings of the National Academy of Sciences; June 2005;102(27):9673–8. Retrieved from: https://doi.org/10.1073%2Fpnas.0504136102

23. Zhan L, Jenkins LM, Wolfson OE, GadElkarim JJ, Nocito K, Thompson PM, et al. The significance of negative correlations in brain connectivity. Journal of Comparative Neurology [Internet]. Wiley; July 2017;525(15):3251–65. Retrieved from: https://doi.org/10.1002%2Fcne.24274

24. Parente F, Frascarelli M, Mirigliani A, Fabio FD, Biondi M, Colosimo A. Negative functional brain networks. Brain Imaging and Behavior [Internet]. Springer Nature; March 2017;12(2):467–76. Retrieved from: https://doi.org/10.1007%2Fs11682-017-9715-x

25. Kelly AMC, Uddin LQ, Biswal BB, Castellanos FX, Milham MP. Competition between functional brain networks mediates behavioral variability. NeuroImage [Internet]. Elsevier BV; January 2008;39(1):527–37. Retrieved from: https://doi.org/10.1016%2Fj.neuroimage.2007.08.008

26. Fortunato S. Community detection in graphs. Physics Reports [Internet]. Elsevier BV; February 2010;486(3-5):75–174. Retrieved from: https://doi.org/10.1016%2Fj.physrep.2009.11.002

27. Sporns O, Betzel RF. Modular Brain Networks. Annual Review of Psychology [Internet]. Annual Reviews; January 2016;67(1):613–40. Retrieved from: https://doi.org/10.1146%2Fannurev-psych-122414-033634

28. Blondel VD, Guillaume J-L, Lambiotte R, Lefebvre E. Fast unfolding of communities in large networks. Journal of Statistical Mechanics: Theory and Experiment [Internet]. IOP Publishing; October

2008;2008(10):P10008. Retrieved from: https://doi.org/10.1088%2F1742-5468%2F2008%2F10%2Fp10008

29. Lancichinetti A, Fortunato S. Community detection algorithms: A comparative analysis. Physical Review E [Internet]. American Physical Society (APS); November 2009;80(5). Retrieved from: https://doi.org/10.1103%2Fphysreve.80.056117

30. Girvan M, Newman MEJ. Community structure in social and biological networks. Proceedings of the National Academy of Sciences [Internet]. Proceedings of the National Academy of Sciences; June 2002;99(12):7821–6. Retrieved from: https://doi.org/10.1073%2Fpnas.122653799

31. Gómez S, Jensen P, Arenas A. Analysis of community structure in networks of correlated data. Physical Review E [Internet]. American Physical Society (APS); July 2009;80(1). Retrieved from: https://doi.org/10.1103%2Fphysreve.80.016114

32. Rubinov M, Sporns O. Weight-conserving characterization of complex functional brain networks. NeuroImage [Internet]. Elsevier BV; June 2011;56(4):2068–79. Retrieved from: https://doi.org/10.1016%2Fj.neuroimage.2011.03.069

33. Traag VA, Bruggeman J. Community detection in networks with positive and negative links. Physical Review E [Internet]. American Physical Society (APS); September 2009;80(3). Retrieved from: https://doi.org/10.1103%2Fphysreve.80.036115

34. Bazzi M, Porter MA, Williams S, McDonald M, Fenn DJ, Howison SD. Community Detection in Temporal Multilayer Networks with an Application to Correlation Networks. Multiscale Modeling & Simulation [Internet]. Society for Industrial & Applied Mathematics (SIAM); January 2016;14(1):1–41. Retrieved from: https://doi.org/10.1137%2F15m1009615

35. MacMahon M, Garlaschelli D. Community Detection for Correlation Matrices. Physical Review X [Internet]. American Physical Society (APS); April 2015;5(2). Retrieved from: https://doi.org/10.1103%2Fphysrevx.5.021006

36. Almog A, Roethler O, Buijink R, Michel S, Meijer JH, Rohling JHT, et al. Uncovering hidden functional brain organization by random matrix theory. arXiv preprint arXiv:170807046. 2017;

37. Van EDC, Smith SM, Barch DM, Behrens TE, Yacoub E, Ugurbil K. The WU-Minn Human Connectome Project: an overview.. Neuroimage. 2013;80:62–79.

38. Uğurbil K, Xu J, Auerbach EJ, Moeller S, Vu AT, Duarte-Carvajalino JM, et al. Pushing spatial and temporal resolution for functional and diffusion MRI in the Human Connectome Project.. Neuroimage. 2013;80:80–104.

39. Glasser MF, Smith SM, Marcus DS, Andersson JLR, Auerbach EJ, Behrens TEJ, et al. The Human Connectome Project's neuroimaging approach. Nature Neuroscience [Internet]. Springer Nature; September 2016;19(9):1175–87. Retrieved from: https://doi.org/10.1038%2Fnn.4361

40. Jeub LGS, Sporns O, Fortunato S. Multiresolution Consensus Clustering in Networks.. Sci Rep. 2018;8:3259.

41. Lancichinetti A, Fortunato S. Consensus clustering in complex networks. Scientific Reports [Internet]. Springer Nature; March 2012;2(1). Retrieved from: https://doi.org/10.1038%2Fsrep00336

42. Glasser MF, Coalson TS, Robinson EC, Hacker CD, Harwell J, Yacoub E, et al. A multi-modal parcellation of human cerebral cortex. Nature [Internet]. Springer Nature; July 2016;536(7615):171–8. Retrieved from: https://doi.org/10.1038%2Fnature18933

43. Bassett DS, Porter MA, Wymbs NF, Grafton ST, Carlson JM, Mucha PJ. Robust detection of dynamic community structure in networks. Chaos: An Interdisciplinary Journal of Nonlinear Science [Internet]. AIP Publishing; March 2013;23(1):013142. Retrieved from: https://doi.org/10.1063%2F1.4790830

44. Honey CJ, Kotter R, Breakspear M, Sporns O. Network structure of cerebral cortex shapes functional connectivity on multiple time scales. Proceedings of the National Academy of Sciences [Internet]. Proceedings of the National Academy of Sciences; June 2007;104(24):10240–5. Retrieved from: https://doi.org/10.1073%2Fpnas.0701519104

45. Mišić B, Betzel RF, Reus MA de, Heuvel MP van den, Berman MG, McIntosh AR, et al. Network-Level Structure-Function Relationships in Human Neocortex. Cerebral Cortex [Internet]. Oxford University Press (OUP); April 2016;26(7):3285–96. Retrieved from: https://doi.org/10.1093%2Fcercor%2Fbhw089

46. Hermundstad AM, Brown KS, Bassett DS, Aminoff EM, Frithsen A, Johnson A, et al. Structurally-Constrained Relationships between Cognitive States in the Human Brain. Hilgetag CC, editor. PLoS Computational Biology [Internet]. Public Library of Science (PLoS); May 2014;10(5):e1003591. Retrieved from: https://doi.org/10.1371%2Fjournal.pcbi.1003591

47. Hric D, Darst RK, Fortunato S. Community detection in networks: Structural communities versus ground truth. Physical Review E [Internet]. American Physical Society (APS); December 2014;90(6). Retrieved from: https://doi.org/10.1103%2Fphysreve.90.062805

48. Betzel RF, Medaglia JD, Bassett DS. Diversity of meso-scale architecture in human and non-human connectomes. Nature Communications [Internet]. Springer Nature; January 2018;9(1). Retrieved from: https://doi.org/10.1038%2Fs41467-017-02681-z

49. Kong R, Li J, Orban C, Sabuncu MR, Liu H, Schaefer A, et al. Spatial Topography of Individual-Specific Cortical Networks Predicts Human Cognition Personality and Emotion. Cold Spring Harbor Laboratory; November 2017; Retrieved from: https://doi.org/10.1101%2F213041

50. Felleman DJ, Essen DCV. Distributed Hierarchical Processing in the Primate Cerebral Cortex. Cerebral Cortex [Internet]. Oxford University Press (OUP); January 1991;1(1):1–47. Retrieved from: https://doi.org/10.1093%2Fcercor%2F1.1.1

51. Andrews-Hanna JR, Reidler JS, Sepulcre J, Poulin R, Buckner RL. Functional-Anatomic Fractionation of the Brain's Default Network. Neuron [Internet]. Elsevier BV; February 2010;65(4):550–62. Retrieved from: https://doi.org/10.1016%2Fj.neuron.2010.02.005

52. Uddin LQ. Salience processing and insular cortical function and dysfunction.. Nat Rev Neurosci. 2015;16:55–61.

53. Betzel RF, Medaglia JD, Papadopoulos L, Baum GL, Gur R, Gur R, et al. The modular organization of human anatomical brain networks: Accounting for the cost of wiring. Network Neuroscience [Internet]. MIT Press - Journals; February 2017;1(1):42–68. Retrieved from: https://doi.org/10.1162%2Fnetn_a_00002

54. Power JD, Schlaggar BL, Petersen SE. Studying Brain Organization via Spontaneous fMRI Signal. Neuron [Internet]. Elsevier BV; November 2014;84(4):681–96. Retrieved from: https://doi.org/10.1016%2Fj.neuron.2014.09.007

55. Betzel RF, Mišić B, He Y, Rumschlag J, Zuo X-N, Sporns O. Functional brain modules reconfigure at multiple scales across the human lifespan. arXiv preprint arXiv:151008045. 2015;

56. Ashourvan A, Telesford QK, Verstynen T, Vettel JM, Bassett DS. Multi-scale detection of hierarchical community architecture in structural and functional brain networks. arXiv preprint arXiv:170405826. 2017;

57. Schaefer A, Kong R, Gordon EM, Laumann TO, Zuo X-N, Holmes AJ, et al. Local-Global Parcellation of the Human Cerebral Cortex from Intrinsic Functional Connectivity MRI. Cerebral Cortex [Internet]. Oxford University Press (OUP); July 2017;:1–20. Retrieved from: https://doi.org/10.1093%2Fcercor%2Fbhx179

58. Gordon EM, Laumann TO, Adeyemo B, Huckins JF, Kelley WM, Petersen SE. Generation and Evaluation of a Cortical Area Parcellation from Resting-State Correlations.. Cereb Cortex. 2016;26:288–303.

59. Buckner RL, Krienen FM, Castellanos A, Diaz JC, Yeo BTT. The organization of the human cerebellum estimated by intrinsic functional connectivity. Journal of Neurophysiology [Internet]. American Physiological Society; November 2011;106(5):2322–45. Retrieved from: https://doi.org/10.1152%2Fjn.00339.2011

60. Choi EY, Yeo BTT, Buckner RL. The organization of the human striatum estimated by intrinsic functional connectivity. Journal of Neurophysiology [Internet]. American Physiological Society; October 2012;108(8):2242–63. Retrieved from: https://doi.org/10.1152%2Fjn.00270.2012

61. Reus MA de, Saenger VM, Kahn RS, Heuvel MP van den. An edge-centric perspective on the human connectome: link communities in the brain. Philosophical Transactions of the Royal Society B: Biological Sciences [Internet]. The Royal Society; September 2014;369(1653):20130527–. Retrieved from: https://doi.org/10.1098%2Frstb.2013.0527

62. Moeller S, Yacoub E, Olman CA, Auerbach E, Strupp J, Harel N, et al. Multiband multislice GE-EPI at 7 tesla with 16-fold acceleration using partial parallel imaging with application to high spatial and temporal whole-brain fMRI. Magnetic Resonance in Medicine [Internet]. Wiley; April 2010;63(5):1144–53. Retrieved from: https://doi.org/10.1002%2Fmrm.22361

63. Feinberg DA, Moeller S, Smith SM, Auerbach E, Ramanna S, Glasser MF, et al. Multiplexed Echo Planar Imaging for Sub-Second Whole Brain FMRI and Fast Diffusion Imaging. Valdes-Sosa PA, editor. PLoS ONE [Internet]. Public Library of Science (PLoS); December 2010;5(12):e15710. Retrieved from: https://doi.org/10.1371%2Fjournal.pone.0015710

64. Setsompop K, Gagoski BA, Polimeni JR, Witzel T, Wedeen VJ, Wald LL. Blipped-controlled aliasing in parallel imaging for simultaneous multislice echo planar imaging with reduced g-factor penalty. Magnetic Resonance in Medicine [Internet]. Wiley; August 2011;67(5):1210–24. Retrieved from: https://doi.org/10.1002%2Fmrm.23097

65. Smith SM, Beckmann CF, Andersson J, Auerbach EJ, Bijsterbosch J, Douaud G, et al. Resting-state fMRI in the Human Connectome Project. NeuroImage [Internet]. Elsevier BV; October 2013;80:144–68. Retrieved from: https://doi.org/10.1016%2Fj.neuroimage.2013.05.039

66. Glasser MF, Sotiropoulos SN, Wilson JA, Coalson TS, Fischl B, Andersson JL, et al. The minimal preprocessing pipelines for the Human Connectome Project. NeuroImage [Internet]. Elsevier BV; October 2013;80:105–24. Retrieved from: https://doi.org/10.1016%2Fj.neuroimage.2013.04.127

67. Griffanti L, Salimi-Khorshidi G, Beckmann CF, Auerbach EJ, Douaud G, Sexton CE, et al. ICA-based artefact removal and accelerated fMRI acquisition for improved resting state network imaging. NeuroImage [Internet]. Elsevier BV; July 2014;95:232–47. Retrieved from: https://doi.org/10.1016%2Fj.neuroimage.2014.03.034

68. Salimi-Khorshidi G, Douaud G, Beckmann CF, Glasser MF, Griffanti L, Smith SM. Automatic denoising of functional MRI data: Combining independent component analysis and hierarchical fusion of classifiers. NeuroImage [Internet]. Elsevier BV; April 2014;90:449–68. Retrieved from: https://doi.org/10.1016%2Fj.neuroimage.2013.11.046

69. Jenkinson M, Bannister P, Brady M, Smith S. Improved optimization for the robust and accurate linear registration and motion correction of brain images.. Neuroimage. 2002;17:825–41.

70. Jenkinson M, Beckmann CF, Behrens TEJ, Woolrich MW, Smith SM. FSL. NeuroImage [Internet]. Elsevier BV; August 2012;62(2):782–90. Retrieved from: https://doi.org/10.1016%2Fj.neuroimage.2011.09.015

71. Fischl B. FreeSurfer. NeuroImage [Internet]. Elsevier BV; August 2012;62(2):774–81. Retrieved from: https://doi.org/10.1016%2Fj.neuroimage.2012.01.021

72. Jeub LGS, Bazzi M, Jutla IS, Mucha PJ. A generalized Louvain method for community detection implemented in MATLAB. 2011-2017; Retrieved from: http://netwiki.amath.unc.edu/GenLouvain

73. Fortunato S, Barthelemy M. Resolution limit in community detection. Proceedings of the National Academy of Sciences [Internet]. Proceedings of the National Academy of Sciences; December 2006;104(1):36–41. Retrieved from: https://doi.org/10.1073%2Fpnas.0605965104

74. Traag VA, Dooren PV, Nesterov Y. Narrow scope for resolution-limit-free community detection. Physical Review E [Internet]. American Physical Society (APS); July 2011;84(1). Retrieved from: https://doi.org/10.1103%2Fphysreve.84.016114

75. Reichardt J, Bornholdt S. Statistical mechanics of community detection. Physical Review E. 2006;74(1):016110.

76. Sales-Pardo M, Guimera R, Moreira AA, Amaral LAN. Extracting the hierarchical organization of complex systems. Proceedings of the National Academy of Sciences [Internet]. Proceedings of the National Academy of Sciences; September 2007;104(39):15224–9. Retrieved from: https://doi.org/10.1073%2Fpnas.0703740104

77. Scannell JW, Burns GA, Hilgetag CC, O'Neil MA, Young MP. The connectional organization of the cortico-thalamic system of the cat.. Cereb Cortex. 1999;9:277–99.

78. Good BH, Montjoye Y-A de, Clauset A. Performance of modularity maximization in practical contexts. Physical Review E [Internet]. American Physical Society (APS); April 2010;81(4). Retrieved from: https://doi.org/10.1103%2Fphysreve.81.046106

79. Traud AL, Kelsic ED, Mucha PJ, Porter MA. Comparing Community Structure to Characteristics in Online Collegiate Social Networks. SIAM Review [Internet]. Society for Industrial & Applied Mathematics (SIAM); January 2011;53(3):526–43. Retrieved from: https://doi.org/10.1137%2F080734315

80. Doron KW, Bassett DS, Gazzaniga MS. Dynamic network structure of interhemispheric coordination. Proceedings of the National Academy of Sciences [Internet]. Proceedings of the National Academy of Sciences; October 2012;109(46):18661–8. Retrieved from: https://doi.org/10.1073%2Fpnas.1216402109

81. Rand WM. Objective Criteria for the Evaluation of Clustering Methods. Journal of the American Statistical Association [Internet]. Informa UK Limited; December 1971;66(336):846–50. Retrieved from: https://doi.org/10.1080%2F01621459.1971.10482356

82. Andersson JLR, Skare S, Ashburner J. How to correct susceptibility distortions in spin-echo echo-planar images: application to diffusion tensor imaging. NeuroImage [Internet]. Elsevier BV; October 2003;20(2):870–88. Retrieved from: https://doi.org/10.1016%2Fs1053-8119%2803%2900336-7

83. Andersson JLR, Sotiropoulos SN. Non-parametric representation and prediction of single- and multi-shell diffusion-weighted MRI data using Gaussian processes. NeuroImage [Internet]. Elsevier BV; November 2015;122:166–76. Retrieved from: https://doi.org/10.1016%2Fj.neuroimage.2015.07.067

84. Andersson JLR, Sotiropoulos SN. An integrated approach to correction for off-resonance effects and subject movement in diffusion MR imaging. NeuroImage [Internet]. Elsevier BV; January 2016;125:1063–78. Retrieved from: https://doi.org/10.1016%2Fj.neuroimage.2015.10.019

85. Yeh F-C, Wedeen VJ, Tseng W-YI. Generalized ${ q}$-Sampling Imaging. IEEE Transactions on Medical Imaging [Internet]. Institute of Electrical and Electronics Engineers (IEEE); September 2010;29(9):1626–35. Retrieved from: https://doi.org/10.1109%2Ftmi.2010.2045126

86. Maier-Hein KH, Neher PF, Houde J-C, Côté M-A, Garyfallidis E, Zhong J, et al. The challenge of mapping the human connectome based on diffusion tractography. Nature Communications [Internet]. Springer Nature; November 2017;8(1). Retrieved from: https://doi.org/10.1038%2Fs41467-017-01285-x

87. Yeh F-C, Verstynen TD, Wang Y, Fernández-Miranda JC, Tseng W-YI. Deterministic Diffusion Fiber Tracking Improved by Quantitative Anisotropy. Zhan W, editor. PLoS ONE [Internet]. Public Library

of Science (PLoS); November 2013;8(11):e80713. Retrieved from: https://doi.org/10.1371%2Fjournal.pone.0080713

88. Wei K, Cieslak M, Greene C, Grafton ST, Carlson JM. Sensitivity analysis of human brain structural network construction. Network Neuroscience [Internet]. MIT Press - Journals; December 2017;1(4):446–67. Retrieved from: https://doi.org/10.1162%2Fnetn_a_00025

89. Hagmann P, Cammoun L, Gigandet X, Meuli R, Honey CJ, Wedeen VJ, et al. Mapping the Structural Core of Human Cerebral Cortex. Friston KJ, editor. PLoS Biology [Internet]. Public Library of Science (PLoS); July 2008;6(7):e159. Retrieved from: https://doi.org/10.1371%2Fjournal.pbio.0060159

90. BETZEL RICHARDF, GRIFFA ALESSANDRA, AVENA-KOENIGSBERGER ANDREA, GOÑI JOAQUIN, THIRAN JEAN-PHILIPPE, HAGMANN PATRIC, et al. Multi-scale community organization of the human structural connectome and its relationship with resting-state functional connectivity. Network Science [Internet]. Cambridge University Press (CUP); December 2013;1(03):353–73. Retrieved from: https://doi.org/10.1017%2Fnws.2013.19

91. Guimerà R, Sales-Pardo M, Amaral LAN. Modularity from fluctuations in random graphs and complex networks. Physical Review E [Internet]. American Physical Society (APS); August 2004;70(2). Retrieved from: https://doi.org/10.1103%2Fphysreve.70.025101

92. Barch DM, Burgess GC, Harms MP, Petersen SE, Schlaggar BL, Corbetta M, et al. Function in the human connectome: Task-fMRI and individual differences in behavior. NeuroImage [Internet]. Elsevier BV; October 2013;80:169–89. Retrieved from: https://doi.org/10.1016%2Fj.neuroimage.2013.05.033

93. Woolrich MW, Ripley BD, Brady M, Smith SM. Temporal Autocorrelation in Univariate Linear Modeling of FMRI Data. NeuroImage [Internet]. Elsevier BV; December 2001;14(6):1370–86. Retrieved from: https://doi.org/10.1006%2Fnimg.2001.0931

94. Binder JR, Gross WL, Allendorfer JB, Bonilha L, Chapin J, Edwards JC, et al. Mapping anterior temporal lobe language areas with fMRI: A multicenter normative study. NeuroImage [Internet]. Elsevier BV; January 2011;54(2):1465–75. Retrieved from: https://doi.org/10.1016%2Fj.neuroimage.2010.09.048